

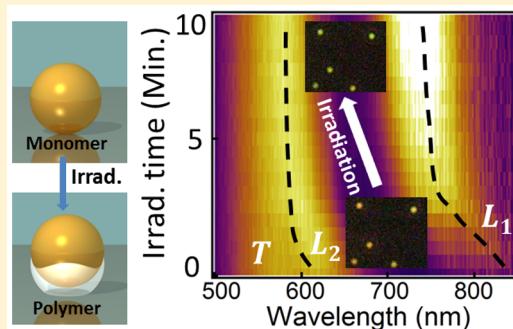
## Light-Directed Tuning of Plasmon Resonances via Plasmon-Induced Polymerization Using Hot Electrons

Tao Ding,<sup>\*,†</sup> Jan Mertens,<sup>†</sup> Anna Lombardi,<sup>†</sup> Oren A. Scherman,<sup>\*,‡,†</sup> and Jeremy J. Baumberg<sup>\*,†</sup><sup>†</sup>Nanophotonics Centre, Cavendish Laboratory, University of Cambridge, Cambridge CB3 0HE, United Kingdom<sup>‡</sup>Melville Laboratory for Polymer Synthesis, Department of Chemistry, University of Cambridge, Lensfield Road, Cambridge CB2 1EW, United Kingdom

## Supporting Information

**ABSTRACT:** The precise morphology of nanoscale gaps between noble-metal nanostructures controls their resonant wavelengths. Here we show photocatalytic plasmon-induced polymerization can locally enlarge the gap size and tune the plasmon resonances. We demonstrate light-directed programmable tuning of plasmons can be self-limiting. Selective control of polymer growth around individual plasmonic nanoparticles is achieved, with simultaneous real-time monitoring of the polymerization process in situ using dark-field spectroscopy. Even without initiators present, we show light-triggered chain growth of various monomers, implying plasmon initiation of free radicals via hot-electron transfer to monomers at the Au surface. This concept not only provides a programmable way to fine-tune plasmons for many applications but also provides a window on polymer chemistry at the sub-nanoscale.

**KEYWORDS:** plasmons, gold, hot electrons, nanoparticles, films, photocatalysis



Plasmons, composed of oscillations of free electrons on noble-metal surfaces, have triggered the discovery of many new phenomena in nanophotonics over the last two decades, leading to promising applications in surface-enhanced spectroscopies,<sup>1</sup> plasmon-assisted photocatalysis,<sup>2,3</sup> water splitting,<sup>4,5</sup> plasmon-mediated resist exposure,<sup>6–10</sup> plasmonic solar cells,<sup>11</sup> and photothermal therapies.<sup>12</sup> Such effects arise from the localized field enhancements or from plasmon-induced hot carriers.<sup>13,14</sup> It is highly desirable to match the excitation wavelength with plasmon resonances so that optimal enhancement or efficiency can be achieved in these diverse applications. In addition, ultralow-power switching of the resonances fostered by their small optical mode volumes achieved can enable new classes of optoelectronic devices. Two tuning strategies are available: changing the refractive index of spacer layers inside plasmonic gaps or changing the gap size itself. Unfortunately the former strategy has not been effective so far. The combination of plasmonic metals with reconfigurable soft-polymer spacers is thus of great interest, to achieve on-demand tuning of plasmons. Previous tuning methods using either chemical<sup>15–17</sup> or physical<sup>18–20</sup> mechanisms yield less-useful abrupt spectral shifts. More recently, light-assisted tuning has enabled continuous tuning but demands active feedback via in situ monitoring, yielding low throughput.<sup>21–23</sup>

Here we introduce the concept of autonomous and programmed tuning based on plasmon-induced polymerization within the nanogaps, which enables trimming of plasmon resonances to the desired spectral position. Monomer polymerization in a nanogap expands its volume, thereby blue-shifting

the plasmon resonances strongly. As the plasmon shifts away from the excitation wavelength, polymer growth terminates, thus stabilizing the plasmon resonances. Such a self-limiting mechanism makes it possible to program tuning by selecting irradiation wavelength and composition of the monomers. We show this process is generic to a large class of free-radical polymerizations, including also functional electronic polymer materials.

## RESULTS AND DISCUSSION

**Tuning Plasmons with Polymerization.** To set the initial gap, the Au substrate is coated with a thiophenol self-assembled monolayer of thickness 0.6 nm, followed by drop-casting 80 nm of Au nanoparticles (NPs) on top. This Au nanoparticle-on-mirror (NPoM) confines strong optical fields (several hundred times the incident field) within the nanogap.<sup>24</sup> The surface-coupled plasmon mode of such plasmonic structures is exquisitely sensitive to the gap size and contents,<sup>25–28</sup> thus giving a means to tune the nanogap spacing on demand as well as to precisely track the polymer growth around each gold nanoparticle. The initial color of the coupled plasmonic resonance from each NPoM is within 10 nm of 800 nm, showing the high degree of robust construction of this architecture.

Irradiation with 635 nm continuous wave (CW) laser light on these Au NPoMs ( $0.2 \text{ mW}/\mu\text{m}^2$ ) completely immersed in a

Received: March 3, 2017

Published: April 25, 2017

bulk monomer of divinylbenzene (DVB) (Supporting Information (SI), Scheme S1) is found to increase the gap size. This results in a 70 nm spectral blue-shift (from 800 to 730 nm) of the coupled plasmon resonance within 400 s (Figure 1a). As long as the concentration of DVB is larger than

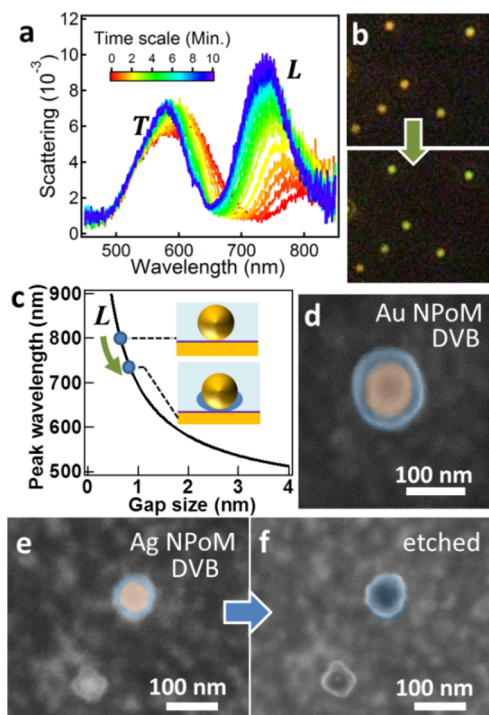


**Figure 1.** Using NPoM plasmon geometry to track light-induced polymerization of DVB. (a) Scattering spectra of Au NP on Au substrate vs irradiation time (635 nm 0.2 mW pump). *T*: transverse mode; *L*: dipolar mode. (b) Dark-field images of Au NPoMs before/after irradiation of entire area. (c) Circuit model prediction of coupled plasmon resonance ( $\lambda_L$ ) vs gap size. Inset depicts polymer growth in the gap between Au NP and Au substrate. (d) SEM image of irradiated Au NPoM in DVB showing PDVB coating. (e, f) SEM images of irradiated Ag NPoM in DVB before/after etching Ag NPs with ammonia. Images are false-colored to highlight core-shell structure.

20% by volume, polymer growth is observed. While, normally, increasing the dielectric constant in the gap results in a plasmon red-shift, here changes in the refractive index of  $<0.05$  induce only small shifts. What instead dominates the spectral shift is the thickness growth of the polymer layer inside the gap. We thus see an overall blue-shift, as the coupled resonances are much more sensitive to the gap separation for such small gaps. The resulting blue-shift overwhelms any potential red-shift from the dielectric increase. Dark-field images of the samples recorded with a CCD camera before and after irradiation reveal a clear change of each nanoparticle-on-mirror scattering color from orange to green (Figure 1b). The scanning electron microscopy (SEM) images of irradiated Au NPoMs further verify the formation of a polymer coating around each AuNP (Figure 1c). As it is beyond current capabilities to directly visualize changes of sub-nanometer gaps (even using FIB/TEM),<sup>20</sup> we use optical spectroscopy to identify the increase in gap size by applying a simple analysis of the plasmon modes.<sup>29</sup> Exact simulations based on finite-difference time-domain simulations have been used to develop a simple model for such plasmonic gaps, which is based on modeling the system as an electrical circuit with inductors and capacitors set by the

geometry of the nanoparticle and its facets.<sup>29,30</sup> Previous work with different spacers and nanoparticle diameters has shown this to be in close agreement with the exact electromagnetic simulations.

The experimentally obtained resonance positions (points in Figure 1c) reveal that the formation of the polymer polydivinylbenzene (PDVB) in the gap increases the distance of the Au NP to the underlying Au substrate from  $0.6 \pm 0.2$  nm to  $0.9 \pm 0.2$  nm. However, since the shell thickness of PDVB around the rest of the Au can be as large as 20 nm (Figure 1d), this shows that polymer growth around the Au NPs is not homogeneous (inset in Figure 1c) but much smaller at the base, where it is in contact with the substrate. This is likely because the monomer is tightly constrained within the gap region, while polymer chain growth is relatively easy from the Au NP surface just outside the immediate vicinity of the gap. This is seen as well when using nanoparticles made from silver, which can also be used for the polymerization (Figure 1e) and which can be subsequently selectively removed using ammonia. Etching the silver leaves behind a polymer feature that seems to replicate the bottom facet of the Ag NPs (Figure 1f).

The laser we use is linearly polarized, but no polarization-dependent growth is observed. This is expected since the cavity modes are actually *z*-polarized.<sup>24,29,30</sup> Our incident laser beam contains both *s*- and *p*-polarized components, as it is focused using an NA = 0.8 objective. While the transverse modes are then also excited, the in-plane field enhancements for generating hot electrons are weaker by more than an order of magnitude,<sup>31</sup> which is why polymerization takes place only in the gap between particle and surface.

We find this method of optically induced polymer coating also applies to hydrophilic monomers such as *N*-isopropylacrylamide (NIPAM) (Figure 2). Dark-field images reveal the gradual change of scattering color of individual Au NPoMs as irradiation proceeds (Figure 2a).

Depending on the exact NP morphology, resonances can change drastically. Here we can see two coupled plasmonic modes (dipolar and quadrupolar) due to a larger lower facet of the Au NP (Figure 2b).<sup>32</sup> The scattering spectra for NIPAM monomers also show the quadrupolar mode blue-shifting from 690 nm to 600 nm when illuminated (Figure 2b). This suggests

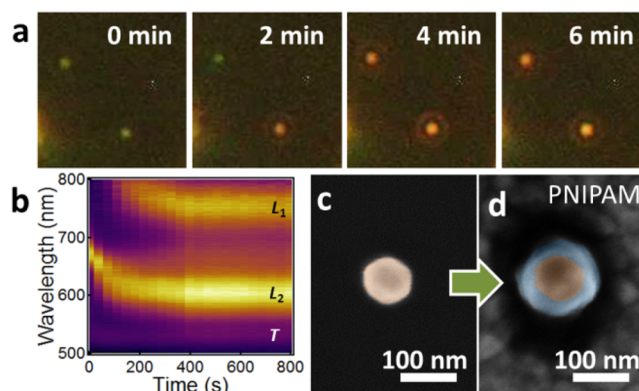
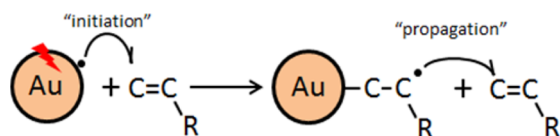


**Figure 2.** Using NPoM plasmon geometry to track light-induced polymerization of NIPAM. Monomer is 2 M, containing 10 wt % *N,N'*-methylenebisacrylamide. (a) Dark-field images and (b) scattering spectra change with increasing irradiation time (635 nm, 0.2 mW pump). Modes *T* = transverse; *L*<sub>1</sub> = dipolar; *L*<sub>2</sub> = quadrupolar. (c, d) SEM images (false color) of Au NPoM (c) before and (d) after irradiation.

an increase of gap size to 2 nm when carefully comparing to our electromagnetic simulations, which have been calibrated against known gap spacings.<sup>27,29,30</sup> The SEM images before and after the polymerization also clearly indicate a coating of PNIPAM around the AuNP. As this monomer does not undergo thermal autoinitiation (and no initiator is added), this gives further support to our claim that hot-electron-assisted polymerization is the mechanism that is responsible (see below).

**Polymerization Process.** Our data confirm that a radical polymerization process takes place around the Au NPoM during the irradiation (also supported by the Raman spectra of the polymers observed after irradiation, SI, Figure S1). We stress that no initiators are used (needed to provide the first radical to start the chain reaction), and at the mW laser powers here, temperature rises of less than 30 °C are produced with this laser wavelength (confirmed by Stokes/anti-Stokes Raman measurements, SI, Figure S2),<sup>33</sup> much less than required for any thermal autoinitiation (>80 °C for most monomers).<sup>7</sup> Therefore, such polymerization seems to be caused by the plasmons. Several mechanisms have been suggested previously including plasmon resonance energy transfer<sup>34,35</sup> or plasmon-induced charge transfer, which shuttles hot electrons or holes from the metal surface layers.<sup>36,37</sup> As photoexcited carriers in the Au are given energies of <2 eV, this is insufficient to directly initiate polymerization (which requires ultraviolet photons), through any possible field-enhanced energy transfer. Different to previous plasmon chemistries<sup>36,38</sup> instead here we suggest the initiation is via hot electrons, not through a redox reaction route, but through formation of  $[\text{Au}-\text{C}-\dot{\text{C}}]$  species near the metal surface, which induces further polymer chain growth (Scheme 1 and SI, Scheme S2). Formation of Au–C bonds is

**Scheme 1. Hot-Electron Initiation Mechanism**



identified in a number of previous reports<sup>39,40</sup> and plausible in our case, although physical attachment is also possible.<sup>41</sup> We find the thickest shells around these Au NPs (Figure 1d) are formed from irradiating DVB monomers, which indicates a reduced chain termination rate arising when PDVB cross-links, which comes from the sterics of this polymerization that reduces the chances of two radical chain-ends meeting. The polymerization process is thus initiated by electrons hopping onto monomers at the Au surface only, followed by radical chain polymerization zipping up each long chain up to a certain distance away where termination occurs.

This hot-electron-mediated radical initiation mechanism implies that irradiation in the presence of any monomers that can be radically polymerized should be able to expand the nanogaps in Au NPoMs and blue-shift the plasmon resonances. Therefore, we test on a range of monomers and directly watch in real time the progression of polymerization from the spectral shifts of the coupled plasmon mode (Figure 3). Molecules containing vinyl bonds (which are polymerizable) lead to blue-shifts of the coupled plasmons after irradiation, although the shift extent is different for different monomers (Figure 3f). We suggest this is due to a difference in radical chain termination rates, which results in different polymer chain lengths. By contrast, no blue-shift is observed (i.e., no polymerization is present in the gap) for small molecules that do not contain vinyl bonds, such as ethylbenzene (EB) (Figure 3e). This verifies that the shells around the Au NPs are indeed made of polymers rather than carbonization products of small organic molecules. Alongside these blue-shifts the scattering intensity also increases, which is due to the decreasing residual intraband absorption of Au at longer wavelength (700–800 nm) as the plasmon shifts to higher energy. We also find the preparation of functional electronic materials such as P3HT is possible using this route, although the mechanism still needs further clarification (SI Figure S3).

**Wavelength-Controlled Feedback.** Since the polymerization process is closely related to the efficiency of hot-electron injection, it is optimal to excite the system close to its coupled plasmon resonance. However, the shifts of the plasmon

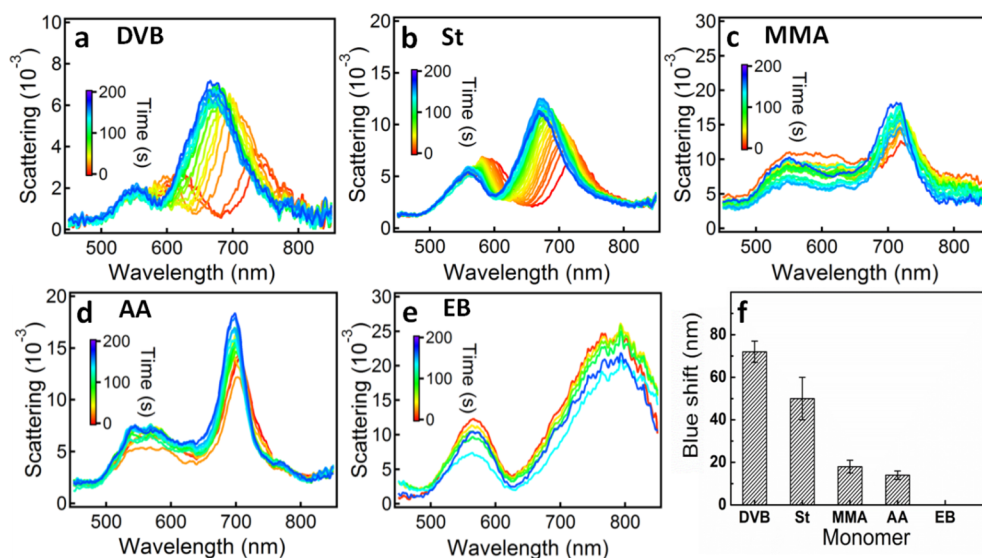


**Figure 3.** Polymerization in different monomers tracked by scattering spectra of Au NPoM. (a–e) Irradiation in monomers of (a) DVB, (b) styrene (St), (c) methyl methacrylate (MMA), (d) acrylic acid (AA), and (e) control with ethylbenzene (EB), which is not polymerizable. Laser on for 200 s, 635 nm, 0.2 mW. (f) Maximum spectral blue-shift of the coupled plasmon for different monomers; error bars show a range of trials.

resonance due to polymerization modify the spectral match between laser wavelength and coupled plasmonic resonance during the irradiation. Actively tracking the plasmon shift using a tunable optical parametric oscillator (OPO) laser source avoids this problem so that the hot-electron generation remains maximized. We observe a continuous blue-shift of the coupled plasmonic resonance from 760 nm to 680 nm ( $\sim 80$  nm shift) using an irradiation laser wavelength that is tuned to follow the plasmon mode from 780 nm down to 633 nm while keeping the power constant at  $10 \mu\text{W}$  (average power, 200 fs pulses) (Figure 4a). The extracted spectral blue-shifts with irradiation

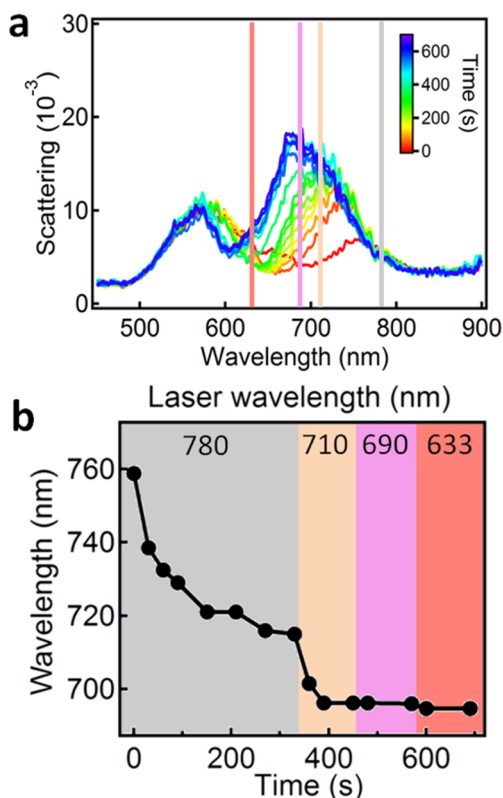


**Figure 4.** Laser-guided polymer growth using tunable excitation wavelengths. (a) Evolving scattering spectra of Au NPoM in DVB as the OPO excitation wavelength is shifted from 780 nm to 633 nm,  $10 \mu\text{W}$  power. (b) Evolution of coupled plasmon wavelength with irradiation time when shifting pump laser wavelength as marked.

time depict the polymerization process in time (Figure 4b). Initially, a 780 nm laser illuminates a single nanoparticle possessing a coupled plasmon mode at 760 nm. The plasmon peak gradually blue-shifts and eventually saturates at 718 nm. This saturation arises because the coupled plasmon moves outside the excitation range of the 780 nm laser and is no longer optically excited, thus turning off the generation of hot electrons for polymerization. When the laser is retuned to 710 nm to again match the coupled plasmon, a new cycle of growth and blue-shifting starts and saturates when the coupled plasmon shifts to 680 nm. Further irradiation with 690 and 633 nm laser light repeats this effect, although smaller blue-shifts are now observed. The smaller shifts at later stages likely arise because of the weakened electric field concentration in the enlarged gap spacing, which gives less efficient hot-electron generation. This self-limiting resonance shift corresponds to less polymer growth under the NP than around its sides, which

again implicates hot-electron initiation that occurs only close to the Au surface. We suggest that in this restricted geometry within the gap there is a higher probability of radical–radical termination reactions, keeping chains short. Our observations demonstrate that this type of plasmon-resonant optically controlled growth mechanism allows us to fine-tune the polymer deposition by using different irradiation wavelengths. Changing the monomer alters both the polymerization rate and the rate at which the plasmon resonance shifts away from the laser via the increasing gap size, creating a unique cycle of feedback that offers selective control of the growth. Thus, we can program the tuning path and allow it to complete at every plasmonic nanostructure.

## CONCLUSIONS

In summary, we have realized light-directed tuning of coupled plasmons by expanding the nanogaps through in situ polymerization. We characterized this using real-time dark-field microscopy on individual and many-nanoparticle constructs. The polymerization process is identified in SEM images and works for both styrenic and acrylic monomers. This method not only can be used to remotely fine-tune the plasmons of NPoM nanostructures in a facile way but also allows the polymer growth to be controlled and monitored with light in real time. Although not suited for mass production of polymers, this method is extremely versatile for synthesis in nanodevices combining selective local synthesis, fine-tuning of sizes ( $<10$  nm), and monitoring by optical spectroscopy. Its generality for different monomers further confirms such polymerization is due to the injection of hot electrons generated by plasmons. This plasmon-mediated process allows light-guided and self-limiting growth of polymers around Au NPs, since the overlap of excitation wavelength with the coupled-plasmon mode determines the efficiency of hot-electron generation, thereby realizing programmable and autonomous tuning of plasmons. Moreover, the mechanism of plasmon-induced polymerization suggested here opens opportunities for developing plasmonic chemistry, examining the details of different polymerizations, as well as for plasmon-tuning devices for sensing applications.

## METHODS

**Nanoassembly.** Gold or silver nanoparticles (Au NPs or Ag NPs, 80 nm diameter, obtained from BBI) are drop-cast on thiophenol self-assembled monolayer (SAM) functionalized gold films (100 nm thick, thermally evaporated). Monomers (with inhibitors removed using 10 wt % NaOH solution) or ethylbenzene ( $10 \mu\text{L}$ ) are then drop-cast onto the samples, which are subsequently covered with a coverslip to provide a flat upper surface for microscope observation (SI, Scheme S1). The widely spatially separated nanoconstructs produced are formed from individual nanoparticles spaced by the thin 0.6 nm thick SAM above the Au mirror. This nanoparticle-on-mirror construct forms robust, highly confined localized plasmons.

**Laser Irradiation.** A 635 nm linearly polarized laser (Coherent Cube) is coupled to the microscope using a single-mode fiber (P3-405BPM-FC-2, Thorlabs), which is then focused down onto the nanoparticles through a  $100\times$  objective (Olympus, NA = 0.8). The irradiation duration and power are varied to tailor the polymerization conditions. For laser-wavelength-tuned irradiation, we use an optical parametric oscillator pumped by a Ti:sapphire laser (Spectra Physics

MaiTai delivering 200 fs pulses, 10 nm line width, at 80 MHz repetition rate), which drives the OPO (Spectra Physics Inspire), with average output powers of tens of mW. By means of a tunable optical filter, the average power of the laser beam is kept below 30  $\mu$ W on the sample focal spot.

**Monitoring.** Dark-field scattering spectra on individual nanoconstructs are taken confocally through a 50  $\mu$ m diameter optical fiber coupled to a spectrometer (QE65000, Ocean Optics) during the irradiation process when the laser is temporarily turned off for 5 s. The irradiated particles are tracked and subsequently characterized with scanning electron microscopy (LEO 1530VP, Zeiss) after a few nanometers of Pt coating. The etching of Ag is performed by immersing the substrate in ammonia solution (25 wt %) for 10 min at ambient conditions.

**Simulations.** Calculation of the gap sizes is performed as follows. Our simulation model consists of an 80 nm AuNP with a bottom facet of width 30 nm separated from a flat gold surface by a continuous spacer of refractive index  $n_g = 1.6$  and enclosed in a homogeneous medium of refractive index  $n_m = 1.55$ . The facet of the AuNP faces the surface, forming a thin nanocavity, which sustains cavity modes as discussed in refs 25 and 30. In addition to cavity modes, an antenna mode associated with the coupling of the particle to its image in the gold surface is present in the system. The resonance position of this antenna mode is calculated using a circuit model<sup>42</sup> and the system parameters above. Antenna and cavity modes couple strongly, resulting in the formation of new hybrid modes. Calculated gap sizes for the NPoM system are obtained by comparing experimental resonances with calculated antenna–cavity hybrid mode positions.

## ■ ASSOCIATED CONTENT

### Supporting Information

The Supporting Information is available free of charge on the ACS Publications website at DOI: 10.1021/acsphtonic.7b00206.

Experimental setup; proposed polymerization mechanism; Raman spectra of PS formed in the nanogap; Stokes and Anti-Stokes Raman; SEM images of Au NP coated with P3HT (PDF)

## ■ AUTHOR INFORMATION

### Corresponding Authors

\*E-mail: t.ding@whu.edu.cn (T. Ding).

\*E-mail: oas23@cam.ac.uk (O. A. Scherman).

\*E-mail: jjb12@cam.ac.uk (J. J. Baumberg).

### ORCID

Oren A. Scherman: 0000-0001-8032-7166

Jeremy J. Baumberg: 0000-0002-9606-9488

### Author Contributions

T.D. conceived and designed the experiments. T.D. and J.M. performed irradiation, spectral measurements, and SEM characterizations. T.D. and A.L. performed laser-tracked growth. T.D., O.A.S., and J.J.B. discussed and analyzed the data. All the authors contributed to writing of the manuscript.

### Notes

The authors declare no competing financial interest.

Raw data of the figures shown in this paper can be found at <https://doi.org/10.17863/CAM.9237>.

## ■ ACKNOWLEDGMENTS

This research is supported by UK Engineering and Physical Sciences Research Council grants EP/G060649/1 and EP/L027151/1 and ERC grant LINASS 320503. T.D. is a Leverhulme Early Career Fellow and gratefully acknowledges the support of the Leverhulme Trust (ECF-2016-606).

## ■ REFERENCES

- (1) Nie, S.; Emory, S. R. Probing Single Molecules and Single Nanoparticles by Surface-Enhanced Raman Scattering. *Science* **1997**, *275*, 1102–1106.
- (2) Mukherjee, S.; Libisch, F.; Large, N.; Neumann, O.; Brown, L. V.; Cheng, J.; Lassiter, J. B.; Carter, E. A.; Nordlander, P.; Halas, N. J. Hot Electrons Do the Impossible: Plasmon-Induced Dissociation of H<sub>2</sub> on Au. *Nano Lett.* **2013**, *13*, 240–247.
- (3) Pincella, F.; Isozaki, K.; Miki, K. A Visible Light-Driven Plasmonic Photocatalyst. *Light: Sci. Appl.* **2014**, *3*, e133.
- (4) Li, J.; Cushing, S. K.; Zheng, P.; Meng, F.; Chu, D.; Wu, N. Plasmon-Induced Photonic and Energy-Transfer Enhancement of Solar Water Splitting by a Hematite Nanorod Array. *Nat. Commun.* **2013**, *4*, 2651.
- (5) Warren, S. C.; Thimsen, E. Plasmonic Solar Water Splitting. *Energy Environ. Sci.* **2012**, *5*, 5133–5146.
- (6) Ueno, K.; Juodkazis, S.; Shibuya, T.; Yokota, Y.; Mizeikis, V.; Sasaki, K.; Misawa, H. Nanoparticle Plasmon-Assisted Two-Photon Polymerization Induced by Incoherent Excitation Source. *J. Am. Chem. Soc.* **2008**, *130*, 6928–6929.
- (7) Stamplecoskie, K. G.; Pacioni, N. L.; Larson, D.; Scaiano, J. C. Plasmon-Mediated Photopolymerization Maps Plasmon Fields for Silver Nanoparticles. *J. Am. Chem. Soc.* **2011**, *133*, 9160–9163.
- (8) Zhou, X.; Deeb, C.; Kostcheev, S.; Wiederrecht, G. P.; Adam, P.-M.; Béal, J.; Plain, J.; Gosztola, D. J.; Grand, J.; Félijd, N.; Wang, H.; Vial, A.; Bachelot, R. Selective Functionalization of the Nanogap of a Plasmonic Dimer. *ACS Photonics* **2015**, *2*, 121–129.
- (9) Zhou, X.; Wenger, J.; Viscomi, F. N.; Le Cunff, L.; Béal, J.; Kochtcheev, S.; Yang, X.; Wiederrecht, G. P.; Colas des Francs, G.; Bisht, A. S.; Jradi, S.; Caputo, R.; Demir, H. V.; Schaller, R. D.; Plain, J.; Vial, A.; Sun, X. W.; Bachelot, R. Two-Color Single Hybrid Plasmonic Nanoemitters with Real Time Switchable Dominant Emission Wavelength. *Nano Lett.* **2015**, *15*, 7458–7466.
- (10) Deeb, C.; Bachelot, R.; Plain, J.; Baudrion, A.-L.; Jradi, S.; Bouhelier, A.; Soppera, O.; Jain, P. K.; Huang, L.; Ecoffet, C.; Balan, L.; Royer, P. Quantitative Analysis of Localized Surface Plasmons Based on Molecular Probing. *ACS Nano* **2010**, *4*, 4579–4586.
- (11) Atwater, H. A.; Polman, A. Plasmonics for Improved Photovoltaic Devices. *Nat. Mater.* **2010**, *9*, 205–213.
- (12) Huang, X.; El-Sayed, M. A. Plasmonic Photo-Thermal Therapy (PpT). *Alexandria J. Med.* **2011**, *47*, 1–9.
- (13) Clavero, C. Plasmon-Induced Hot-Electron Generation at Nanoparticle/Metal-Oxide Interfaces for Photovoltaic and Photocatalytic Devices. *Nat. Photonics* **2014**, *8*, 95–103.
- (14) Brongersma, M. L.; Halas, N. J.; Nordlander, P. Plasmon-Induced Hot Carrier Science and Technology. *Nat. Nanotechnol.* **2015**, *10*, 25–34.
- (15) Jin, R.; Cao, Y.; Mirkin, C. A.; Kelly, K. L.; Schatz, G. C.; Zheng, J. G. Photoinduced Conversion of Silver Nanospheres to Nanoprisms. *Science* **2001**, *294*, 1901–1903.
- (16) Pallares, R. M.; Su, X.; Lim, S. H.; Thanh, N. T. K. Fine-Tuning of Gold Nanorod Dimensions and Plasmonic Properties Using the Hofmeister Effects. *J. Mater. Chem. C* **2016**, *4*, 53–61.
- (17) Genç, A.; Patarroyo, J.; Sancho-Parramon, J.; Arenal, R.; Duchamp, M.; Gonzalez, E. E.; Henrard, L.; Bastús, N. G.; Dunin-Borkowski, R. E.; Puentes, V. F.; Arbiol, J. Tuning the Plasmonic Response Up: Hollow Cuboid Metal Nanostructures. *ACS Photonics* **2016**, *3*, 770–779.
- (18) Mock, J. J.; Hill, R. T.; Degiron, A.; Zauscher, S.; Chilkoti, A.; Smith, D. R. Distance-Dependent Plasmon Resonant Coupling

between a Gold Nanoparticle and Gold Film. *Nano Lett.* **2008**, *8*, 2245–2252.

(19) Ding, T.; Herrmann, L. O.; de Nijs, B.; Benz, F.; Baumberg, J. J. Self-Aligned Colloidal Lithography for Controllable and Tuneable Plasmonic Nanogaps. *Small* **2015**, *11*, 2139–2143.

(20) Ameer, F. S.; Varahagiri, S.; Benza, D. W.; Willett, D. R.; Wen, Y.; Wang, F.; Chumanov, G.; Anker, J. N. Tuning Localized Surface Plasmon Resonance Wavelengths of Silver Nanoparticles by Mechanical Deformation. *J. Phys. Chem. C* **2016**, *120*, 20886–20895.

(21) Jung, H.; Cha, H.; Lee, D.; Yoon, S. Bridging the Nanogap with Light: Continuous Tuning of Plasmon Coupling between Gold Nanoparticles. *ACS Nano* **2015**, *9*, 12292–12300.

(22) Ding, T.; Mertens, J.; Sigle, D. O.; Baumberg, J. J. Capillary-Force-Assisted Optical Tuning of Coupled Plasmons. *Adv. Mater.* **2015**, *27*, 6457–6461.

(23) Lumdee, C.; Toroghi, S.; Kik, P. G. Post-Fabrication Voltage Controlled Resonance Tuning of Nanoscale Plasmonic Antennas. *ACS Nano* **2012**, *6*, 6301–6307.

(24) Mertens, J.; Eiden, A. L.; Sigle, D. O.; Huang, F.; Lombardo, A.; Sun, Z.; Sundaram, R. S.; Colli, A.; Tserkezis, C.; Aizpurua, J.; Milana, S.; Ferrari, A. C.; Baumberg, J. J. Controlling Subnanometer Gaps in Plasmonic Dimers Using Graphene. *Nano Lett.* **2013**, *13*, 5033–5038.

(25) Sigle, D. O.; Mertens, J.; Herrmann, L. O.; Bowman, R. W.; Ithurria, S.; Dubertret, B.; Shi, Y.; Yang, H. Y.; Tserkezis, C.; Aizpurua, J.; Baumberg, J. J. Monitoring Morphological Changes in 2D Monolayer Semiconductors Using Atom-Thick Plasmonic Nanocavities. *ACS Nano* **2015**, *9*, 825–830.

(26) Ding, T.; Sigle, D.; Zhang, L.; Mertens, J.; de Nijs, B.; Baumberg, J. Controllable Tuning Plasmonic Coupling with Nanoscale Oxidation. *ACS Nano* **2015**, *9*, 6110–6118.

(27) de Nijs, B.; Bowman, R. W.; Herrmann, L. O.; Benz, F.; Barrow, S. J.; Mertens, J.; Sigle, D. O.; Chikkaraddy, R.; Eiden, A.; Ferrari, A.; Scherman, O. A.; Baumberg, J. J. Unfolding the Contents of Sub-nm Plasmonic Gaps Using Normalising Plasmon Resonance Spectroscopy. *Faraday Discuss.* **2015**, *178*, 185–193.

(28) Hill, R. T.; Mock, J. J.; Hucknall, A.; Wolter, S. D.; Jokerst, N. M.; Smith, D. R.; Chilkoti, A. Plasmon Ruler with Angstrom Length Resolution. *ACS Nano* **2012**, *6*, 9237–9246.

(29) Benz, F.; Tserkezis, C.; Herrmann, L. O.; de Nijs, B.; Sanders, A.; Sigle, D. O.; Pukenas, L.; Evans, S. D.; Aizpurua, J.; Baumberg, J. J. Nanooptics of Molecular-Shunted Plasmonic Nanojunctions. *Nano Lett.* **2015**, *15*, 669–674.

(30) Tserkezis, C.; Esteban, R.; Sigle, D. O.; Mertens, J.; Herrmann, L. O.; Baumberg, J. J.; Aizpurua, J. Hybridization of Plasmonic Antenna and Cavity Modes: Extreme Optics of Nanoparticle-on-Mirror Nanogaps. *Phys. Rev. A: At, Mol., Opt. Phys.* **2015**, *92*, 053811.

(31) Sundararaman, R.; Narang, P.; Jermyn, A. S.; Goddard Iii, W. A.; Atwater, H. A. Theoretical Predictions for Hot-Carrier Generation from Surface Plasmon Decay. *Nat. Commun.* **2014**, *5*, 5788.

(32) Mertens, J.; Demetriadou, A.; Bowman, R. W.; Benz, F.; Kleemann, M. E.; Tserkezis, C.; Shi, Y.; Yang, H. Y.; Hess, O.; Aizpurua, J.; Baumberg, J. J. Tracking Optical Welding through Groove Modes in Plasmonic Nanocavities. *Nano Lett.* **2016**, *16*, 5605–5611.

(33) Govorov, A. O.; Richardson, H. H. Generating Heat with Metal Nanoparticles. *Nano Today* **2007**, *2*, 30–38.

(34) Li, J.; Cushing, S. K.; Meng, F.; Senty, T. R.; Bristow, A. D.; Wu, N. Plasmon-Induced Resonance Energy Transfer for Solar Energy Conversion. *Nat. Photonics* **2015**, *9*, 601–607.

(35) Liu, G. L.; Long, Y.-T.; Choi, Y.; Kang, T.; Lee, L. P. Quantized Plasmon Quenching Dips Nanospectroscopy Via Plasmon Resonance Energy Transfer. *Nat. Methods* **2007**, *4*, 1015–1017.

(36) Minamimoto, H.; Toda, T.; Futashima, R.; Li, X.; Suzuki, K.; Yasuda, S.; Murakoshi, K. Visualization of Active Sites for Plasmon-Induced Electron Transfer Reactions Using Photoelectrochemical Polymerization of Pyrrole. *J. Phys. Chem. C* **2016**, *120*, 16051–16058.

(37) Wu, K.; Chen, J.; McBride, J. R.; Lian, T. Efficient Hot-Electron Transfer by a Plasmon-Induced Interfacial Charge-Transfer Transition. *Science* **2015**, *349*, 632–635.

(38) Liu, F.; Lubber, E. J.; Huck, L. A.; Olsen, B. C.; Buriak, J. M. Nanoscale Plasmonic Stamp Lithography on Silicon. *ACS Nano* **2015**, *9*, 2184–2193.

(39) Batra, A.; Kladnik, G.; Gorjizadeh, N.; Meisner, J.; Steigerwald, M.; Nuckolls, C.; Quek, S. Y.; Cvetko, D.; Morgante, A.; Venkataraman, L. Trimethyltin-Mediated Covalent Gold–Carbon Bond Formation. *J. Am. Chem. Soc.* **2014**, *136*, 12556–12559.

(40) Cheng, Z. L.; Skouta, R.; Vazquez, H.; Widawsky, J. R.; Schneebeli, S.; Chen, W.; Hybertsen, M. S.; Breslow, R.; Venkataraman, L. In Situ Formation of Highly Conducting Covalent Au-C Contacts for Single-Molecule Junctions. *Nat. Nanotechnol.* **2011**, *6*, 353–357.

(41) Bünsow, J.; Mänz, M.; Vana, P.; Johannsmann, D. Electrochemically Induced Raft Polymerization of Thermoresponsive Hydrogel Films: Impact on Film Thickness and Surface Morphology. *Macromol. Chem. Phys.* **2010**, *211*, 761–767.

(42) Benz, F.; de Nijs, B.; Tserkezis, C.; Chikkaraddy, R.; Sigle, D. O.; Pukenas, L.; Evans, S. D.; Aizpurua, J.; Baumberg, J. J. Generalized Circuit Model for Coupled Plasmonic Systems. *Opt. Express* **2015**, *23*, 33255–33269.